Title

Lepidocrocite-type Layered Titanate Structures: New Lithium and Sodium Ion Intercalation Anode Materials

Authors

Shirpour, Mona
Cabana, Jordi
Doeff, Marca

Publication Date

2014-04-15

Lepidocrocite-type Layered Titanate Structures: New Lithium and Sodium Ion Intercalation Anode Materials

Mona Shirpour[a], Jordi Cabana[b], and Marca Doeff[a]

a) Environmental Energy Technologies Division

Lawrence Berkeley National Laboratory

University of California, Berkeley, CA 94720

and

b) Chemistry Department

University of Illinois at Chicago

Chicago, IL 60607

Abstract

The electrochemical characteristics of lepidocrocite-type titanates derived from $K_{0.8}Ti_{1.73}Li_{0.27}O_4$ are presented for the first time. By exchanging sodium ions for potassium, the practical specific capacity of the titanate in both sodium and lithium half cells is considerably enhanced. Although the gross structural features of the titanate framework are maintained during the ion exchange process, the symmetry changes because sodium occupies different sites from potassium. The smaller size of the sodium ion compared to potassium and the change in site symmetry allow more alkali metal cations to be inserted reversibly into the structure during discharge in sodium and lithium cells than in the parent compound. Insertion of lithium cations takes place at an average of about 0.8V vs. Li^+/Li while sodium intercalation occurs at 0.5V vs. Na^+/Na, with sloping voltage profiles exhibited for both cell configurations, implying single-phase processes. *Ex situ* synchrotron X-ray diffraction measurements show that a lithiated

lepidocrocite is formed during discharge in lithium cells, which undergoes further lithium insertion with almost no volume change. In sodium cells, insertion of sodium initially causes an overall expansion of about 12% in the *b* lattice parameter but reversible uptake of solvent minimizes changes upon further cycling. In the case of the sodium cells, both the practical capacity and the cyclability are improved when a more compliant binder (polyacrylic acid) that can accommodate volume changes associated with insertion processes is used in place of the more common polyvinylidene fluoride. The ability to tune the electrochemical properties of lepidocrocite titanate structures by varying compositions and utilizing ion exchange processes make them especially versatile anode materials for both lithium and sodium ion battery configurations.

Keywords: titanate, anode, Na-ion battery, Li-ion battery

Introduction

Layered titanates represent a class of materials whose physical, ion exchange, and electrochemical intercalation properties are of great technological interest. These compounds have found use as fillers,[1] adsorbents for water treatment and nuclear waste cleanup,[2, 3, 4] functional nanosheets[5] and photocatalysts.[6] Several layered titanates have recently been shown to undergo reversible reductive intercalation of both lithium and sodium ions. [7, 8, 9, 10, 11] Some of these electrode materials, which have theoretical capacities in excess of 200 mAh/g, insert alkali metal cations at unusually low potentials (below 0.5V in some cases). These characteristics have important implications for the design of high-energy dual intercalation batteries, particularly when the intercalant is sodium. In fact, the successful demonstration of a high capacity reversible titanate anode will most likely be an enabling technology for the successful development of sodium ion batteries, because of the inability of graphite anodes (commonly used in lithium ion battery configurations) to insert sodium to any appreciable extent. While hard carbon materials have been shown to have a high reversible capacity for sodium,[12] there are legitimate concerns about the safety of these materials. Another valuable feature of the titanates is their higher densities (~3.5 g/cm^3) compared to graphite (2.25 g/cm^3) and other carbon-based electrodes, which also improves the energy density in both lithium ion and sodium ion configurations. Finally, the low cost, nontoxicity, and rich abundance of titanium are also attractive for industrial applications, particularly for large-scale batteries, such as those used for vehicles or grid storage.

Many ternary titanate phases consist of edge- and corner-sharing TiO_6 octahedra that are linked to form stepped layered structures, with cations and, sometimes, water molecules located between the layers. The lengths of the steps and the interlayer spacing vary depending on

stoichiometry and the nature of the guest species. Ion exchange processes using "chimie douce" (soft chemistry) techniques further enables tuning of these structures to prepare bifunctional hybrid materials, crystals with interesting optical and catalytical properties, and new compounds for conduction and ion transport devices such as sensors and fuel cells.[13, 14] In this way, the capability of layered titanates to accommodate a variety of guest species between the layers can be exploited to design new materials with improved properties, such as increased capacity for reductive intercalation processes when used as electrodes in battery systems.

There exist titanates with corrugated layered structures similar to that of the lepidocrocite mineral γ-FeOOH, which are closely related to these stepped layered structures and share many of the physical properties, including the capability for ion exchange. They comprise a large class of isomorphous compounds with composition $A_xTi_{2-y}M_yO_4$, where A= K, Rb, or Cs, and M represents a vacancy or Li, Mg, Co, Ni, Cu, Zn, or Mn.[15, 16, 17, 18] Lepidocrocite titanates usually crystallize in an orthorhombic structure, consisting of two-dimensional layers of edge and corner sharing octahedra with the large alkali metal ions (A) located in the interlayers. These compensate for the negative charges that arise from the substitution of low valency metal ions or vacancies (M) for Ti^{4+}. The values of x and y are directly related to each other by the redox state of M (y=x/4 for a vacancy, y=x/3 for M^{+}, y=x/2 for M^{2+}, and y=x for M^{3+}), so that the number of vacancies in the interlayer spaces can be varied by changing the overall composition of the lepidocrocite titanate. In addition, the interlayer ions in the lepidocrocite structure are highly exchangeable with a variety of inorganic and organic cations. [15, 19, 20] The compositional flexibility and the capability of using low temperature ion exchange methods mean that a variety of compounds with the desired intercalation characteristics can easily be designed.

Herein, we report on the preparation, crystal structure, ion exchange and electrochemical properties of one such lepidocrocite-type layered titanate and materials derived from it as an example of the utility of these structures for battery applications requiring high energy density.

Experimental

Potassium titanate $K_{0.8}Ti_{1.73}Li_{0.27}O_4$ was prepared via a solid-state reaction. A stoichiometric mixture of K_2CO_3 (purity 99+%, Aldrich), TiO_2 (anatase, purity 99.7%, <25 nm, Sigma-Aldrich) and Li_2CO_3 (purity 99+%, Aldrich) was calcined at 800° C for 1h in air. The calcined powder was pressed as a pellet and calcined again at 800° C for 20h in air. The resulting titanate was milled in a planetary mill at 300 rpm for 2 h in acetone. The as-prepared $K_{0.8}Ti_{1.73}Li_{0.27}O_4$ was converted to the sodium form by a direct ion exchange step. 1 g of $K_{0.8}Ti_{1.73}Li_{0.27}O_4$ was stirred in 100 ml (solution/solid=100 cm^3/g) aqueous solution of 4 M NaCl at 80 °C for 6 days in a closed vial. Then it was vacuum filtered, washed and dried at 110°C in a vacuum oven for 20 hours. Phase analysis of the obtained materials was obtained from powder XRD data collected on a Philips PW3040 X'Pert Pro Diffractometer using a Cu Kα (λ=1.54056Å) source operated at 45 keV and equipped with an X'celerator detector. A high-temperature chamber (Anton Paar HTK 1200N) was used for *in situ* XRD measurements (heating rate of 20 °C/min, equilibrium time of 1 hour). The XRD data of the bulk samples were analyzed by the whole pattern method with GSAS[21] using EXPGUI,[22] and CelRef (http://www.ccp14.ac.uk/tutorial/lmgp/celref.htm) was used to obtain the lattice parameters of phases observed during the *in situ* measurements.

The morphology and composition of the samples were analyzed with a scanning electron microscope (JEOL JSM 7500F) equipped with an energy dispersive X-ray spectrometer (EDS)

(Noran system S1X, Thermo Electron Corporation, model 6714A01SUS-SN). In addition, samples were dissolved in HNO_3 aqueous solution and analyzed by inductively coupled plasma atomic emission spectroscopy (ICP-OES, Perkin Elmer Optima 5300 DV). Thermogravimetric analysis (TGA) was performed on a SDT Q600 system in an argon atmosphere at a heating rate of 10 °C/min. Raman spectra were obtained using a Spex 1877 0.6m Triple Spectrometer, coupled to a liquid nitrogen cooled CCD detector (Princeton Instruments) and a Lexel Model 95 Argon Ion Laser at 488 nm and 300 mW.

Ex situ synchrotron XRD measurements were recorded at 12.74 keV at beamline 11-3 at the Stanford Synchrotron Radiation Lightsource (SSRL). The diffracted intensities were recorded on a 2D Mar345 image plate detector with 150× 150 μm^2 pixels with a detector distance of 150 mm from the sample center and 30 s exposure time. The incident beam on the sample was approximately 50×50 μm^2. The detector image was calibrated using a LaB_6 standard powder. Data were internally calibrated using the aluminum diffraction peaks and analyzed with Area Diffraction Machine.[23] For the figures, Q was converted to the equivalent 2θ for Cu Kα for the patterns as a matter of convenience, and CelRef was used to estimate lattice parameters.

Electrochemical characterization was performed in lithium metal and sodium metal half-cell configurations. Prior to electrode preparation in a helium filled glove box, samples were dried at 160 ºC for 12 hours. One sample of the sodium-exchanged material was also dried at 250 ºC for the same length of time prior to evaluation in electrochemical cells. The dried powder and acetylene black (Denka) were milled together in a planetary mill at 300 rpm for 2 hours under argon. The milled batch was mixed with polyvinylidene fluoride (PVdF, 99.5+%, Aldrich) in N-methylpyrrolidone (NMP, Sigma Aldrich) in 70:20:10 (wt/wt) ratio to form a slurry. For the PAA containing electrodes, polyacrylic acid (PAA, Sigma-Aldrich) dissolved in ethanol was

used as a binder instead of PVdF. The slurry was cast onto Cu foil (Pred Materials), for lithium cells, and Al foil (Exopack Advanced Coatings) for sodium cells, and dried in a vacuum oven at 120 °C for 12 hours. The active material mass loading was about 5 g/cm^2. The 2032-type coin cells were assembled inside a helium filled glovebox. Celgard 2400 was used as separators and 1M $LiPF_6$ in EC:DMC (ethylene carbonate: dimethyl carbonate, Novolyte Technologies) and 1M $NaPF_6$ (Sigma Aldrich) in EC:DMC (3:7 mol, from Novolyte Technologies) as the electrolytic solutions for lithium and sodium cells, respectively. Electrochemical evaluation was carried out using a Bio-logic VMP3 potentiostat/galvanostat equipped with electrochemical impedance spectroscopy capabilities. Impedance data were obtained in the frequency range of 20 kHz-20 mHz on selected lithium and sodium half cells prior to cycling and after each half cycle. Cells were allowed to rest for 10 minutes after the galvanostatic experiments before impedance data was collected.

For the *ex situ* synchrotron XRD measurements, cycled coin cells were disassembled inside a helium filled glove box and the charged or discharged electrodes were rinsed with dimethyl carbonate (DMC) and sealed using Kapton tape. For the electrodes cycled in lithium cells, the copper current collector was removed and the electrode was sealed together with aluminum foil as an internal reference.

Results and Discussion

Chemical and Structural Characterization

We adopted a direct ion exchange process to prepare a sodium form of lepidocrocite titanate from a potassium-containing analog ($K_{0.8}Ti_{1.73}Li_{0.27}O_4$) that can be made directly via solid-state reaction. Earlier studies involving the ion exchange properties of this material[15] first used an

acid-exchange step prior to incorporating sodium into the structure. Here, we have modified the procedure and prepared the sodium form of this compound using a one-step ion exchange, in order to avoid the presence of protons in the samples. Our results on materials prepared using an acid-exchange step are given in a previous publication,[24] and a comparison shows that the one-step ion exchange method improves the electrochemical properties. The $K_{0.8}Ti_{1.73}Li_{0.27}O_4$ powders consist of micron-sized particles with a plate-like morphology (Figure 1a) that was maintained after the ion exchange step (Figure 1b). The composition evolution during ion exchange was studied by EDS/SEM and ICP-OES analysis. The EDS patterns in Figure 1c indicate that nearly all the interlayer K^+ ions were extracted and replaced by sodium ions: K/Ti=0.41 for the as-made material compared to K/Ti=0.04 and Na/Ti=0.53 for the sodium ion-exchanged sample. The ICP-OES chemical analysis corroborated these results, giving K/Ti= 0.43 for $K_{0.8}Ti_{1.73}Li_{0.27}O_4$ and K/Ti = 0.01 and Na/Ti=0.50 for the sodiated sample. Based on these experiments, formulas of $K_{0.74}Ti_{1.73}Li_{0.27}O_4$ for the as-made material and $Na_{0.87}Ti_{1.73}Li_{0.27}O_4 \cdot nH_2O$ for the ion-exchanged material were estimated. The slightly high sodium content is most likely due to traces of sodium salt left over from the exchange process on particle surfaces, because reduction of Ti below +4 is not expected under these conditions. These are very close to the nominal compositions of $K_{0.8}Ti_{1.73}Li_{0.27}O_4$ and $Na_{0.8}Ti_{1.73}Li_{0.27}O_4 \bullet nH_2O$ expected for the compounds based on the general stoichiometries for lepidocrocite titanates discussed above, and assuming that a simple ion-exchange process has occurred.

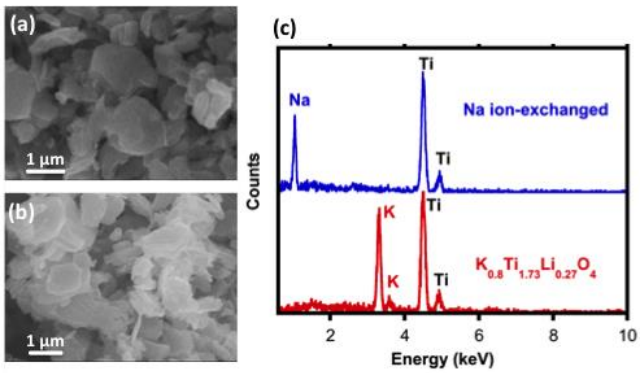

Figure 1. Scanning electron micrographs of (a) $K_{0.8}Ti_{1.73}Li_{0.27}O_4$ and (b) the Na ion-exchanged analog, (c) EDS spectra of $K_{0.8}Ti_{1.73}Li_{0.27}O_4$ (bottom) and the Na ion-exchanged analog (top).

The whole pattern fittings of the XRD patterns of $K_{0.8}Ti_{1.73}Li_{0.27}O_4$ and $Na_{0.8}Ti_{1.73}Li_{0.27}O_4 \bullet nH_2O$ are shown in Figure 2. The profile refinement of the $K_{0.8}Ti_{1.73}Li_{0.27}O_4$ structure in space group *Cmcm* yielded satisfactory fits and matches well with reference 15. The structure of the sodium-substituted phase has not been fully refined, but Sasaki[15] suggested an orthorhombic P-type structure. A structure-less pattern matching using the space group *Pmmm* led to an acceptable fit. The refined unit cell dimensions of both phases are presented in Table 1.

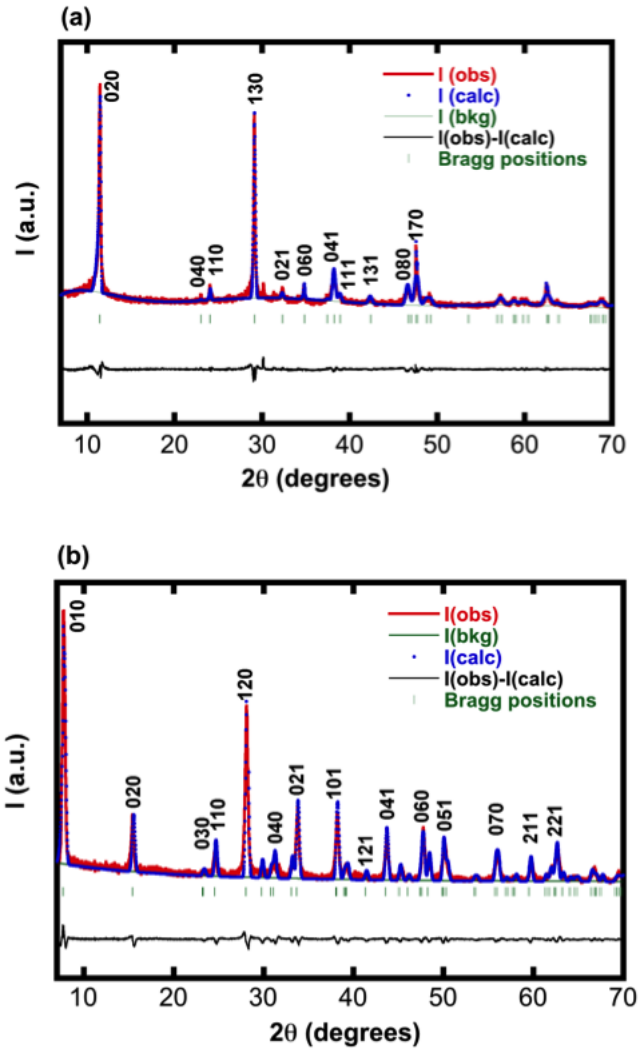

Figure 2. Experimental XRD patterns (solid lines) and calculated patterns (dotted line) of the (a) $K_{0.8}Ti_{1.73}Li_{0.27}O_4$ and (b) Na ion-exchanged samples. The vertical marks indicate the position of Bragg peaks and the bottom line shows the differences between the observed and calculated intensities.

Table 1. Structural parameters for lepidocrocite titanate materials in this study.

Sample	Space group	*a*, Å	*b*, Å	*c*, Å	R_{wp}	Charge density (nm^{-2})
$K_{0.8}Ti_{1.73}Li_{0.27}O_4$	*Cmcm*	3.82	15.50	2.98	9.1	3.51
$Na_{0.8}Ti_{1.73}Li_{0.27}O_4 \bullet nH_2O$ (as-made)	*Pmmm*	3.83	11.52	3.01	9.9	3.47
$Na_{0.8}Ti_{1.73}Li_{0.27}O_4$ (dried at 160 °C)	*Pmmm*	3.80	9.40	3.04	N/A[a]	3.46
$Na_{0.8}Ti_{1.73}Li_{0.27}O_4$ (dried at 250 °C)	*C-type*	3.47	14.57	2.96	N/A[a]	3.90

a. lattice parameters estimated using CelRef.

Polyhedral representations of the two structures are illustrated in Figure 3, based on the refinement results and structural information from the literature cited above.[15] The interlayer cations not only define the dimension along the *b*-axis, but also determine the symmetry of the unit cell. The replacement of K^+ ions by Na^+ ions is accompanied by lateral gliding of the octahedral layers along the *a* axis by *a*/2 with respect to each other. In the $K_{0.8}Ti_{1.73}Li_{0.27}O_4$ structure (*Cmcm* space group) shown in Figure 3 (top), the distance between two of the transition metal layers is equal to *b*/2=7.75 Å. The interlayer distance in the P-type $Na_{0.8}Ti_{1.73}Li_{0.27}O_4 \bullet nH_2O$ structure, in contrast, is equal to the *b* dimension (11.52 Å) because the unit cell contains fewer layers than C-type lepidocrocites like $K_{0.8}Ti_{1.73}Li_{0.27}O_4$. K^+ ions in $K_{0.8}Ti_{1.73}Li_{0.27}O_4$ are accommodated in trigonal prismatic sites shown in Figure 4a (4c positions). Two adjacent sites cannot be occupied simultaneously due to the large size of the ions, resulting in a large number of vacancies in the galleries (occupancy=0.4 for these sites). In the $Na_{0.8}Ti_{1.73}Li_{0.27}O_4 \bullet nH_2O$ structure, oxygen atoms in the adjacent layers face each other and form

cubic cavities in the interlayer galleries (Figure 4b). These large cavities can accommodate more and/or larger cations or neutral species, including hydrated cations and/or water molecules.

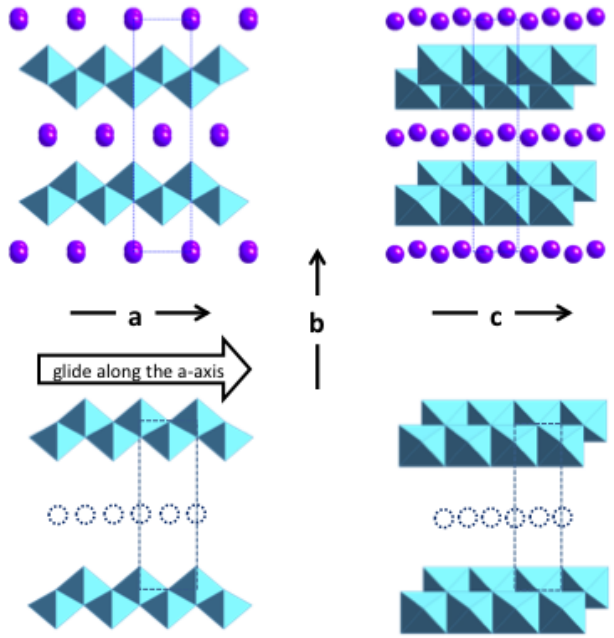

Figure 3. Structure of $K_{0.8}Ti_{1.73}Li_{0.27}O_4$ (space group *Cmcm*) (top) and proposed structural model for the Na ion-exchanged analog (space group *Pmmm*) (bottom). Octahedra are composed of TiO_6 units and spheres indicate K^+ ions and dashed circles indicate possible sites for hydrated Na^+ ions based on the symmetry elements in space group *Pmmm*.

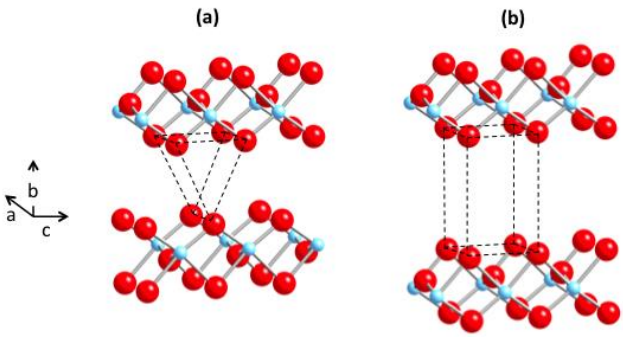

Figure 4. Interlayer sites for the structures depicted in Figure 3: (a) trigonal prismatic in $K_{0.8}Ti_{1.73}Li_{0.27}O_4$ and (b) pseudocubic in the Na ion-exchanged analog.

Also listed in Table 1 is another parameter related to structure, that of the charge density. This is defined as x/2*ac* for $A_xTi_{2-y}M_yO_4$ lepidocrocite structures, where *a* and *c* are unit cell parameters. These values give an indication of the tendency for materials to take up bulky guest species such as large ions, solvents, or water.[16] The value of about 3.5 nm^{-2} for the subject materials in this study suggest that they have a stronger propensity to undergo these processes than $Na_2Ti_3O_7$, which has a charge density of 5.75 nm^{-2}, but weaker than that of smectite clays (~1.7 nm^{-2}), which readily swell and exfoliate in water. The concept of charge density has important implications for the observed physical and electrochemical properties of the lepidocrocites, which will be discussed later.

The presence of interlayer water molecules in $Na_{0.8}Ti_{1.73}Li_{0.27}O_4 \bullet nH_2O$ was confirmed by TG/DTA and *in situ* XRD measurements (Figure 5). The interlayer spacing of 11.52 Å for the as-made $Na_{0.8}Ti_{1.73}Li_{0.27}O_4 \bullet nH_2O$ is typical of a hydrate with a bilayer arrangement of water and cations in the galleries.[15] After heating to 100 ºC, this value decreased to 9.40 Å and was accompanied by a large weight loss. The major portion of the weight loss upon heating, about 23%, was completed by about 150 ºC and corresponded to about 2.8 mol H_2O per

$Na_{0.8}Ti_{1.73}Li_{0.27}O_4 \bullet nH_2O$ formula unit. Upon further heating there was only another 2.4 wt.% weight loss (= 0.2 mol H_2O). This gives an estimate of n=3 in the idealized formula of $Na_{0.8}Ti_{1.73}Li_{0.27}O_4 \bullet nH_2O$. The XRD pattern of the sample heated to 200 °C, showed a further decrease in the interlayer spacing, however, and was consistent with a phase transition to a C-type lepidocrocite structure with a much smaller spacing than $K_{0.8}Ti_{1.73}Li_{0.27}O_4$ (~7.29 Å). Patterns taken at higher temperatures showed that $Na_{0.8}Ti_{1.73}Li_{0.27}O_4 \bullet nH_2O$ ultimately decomposed to phases related to $Na_2Ti_6O_{13}$ and $Na_2Ti_3O_7$.

Based on these results, samples were dried at either 160 or 250 °C. At 160 ºC, a somewhat moisture sensitive P-type lepidocrocite structure with a smaller interlayer spacing than the hydrate is produced. The material dried at 250 ºC is a C-type lepidocrocite and does not take up water or revert to a P-type structure upon cooling. The lattice parameters of these phases are also reported in Table 1. In contrast, the total observed weight loss for the $K_{0.8}Ti_{1.73}Li_{0.27}O_4$ sample upon heating up to 200°C was less than 6%, or about 0.6 mol water per formula unit, and its XRD pattern did not show any changes upon heating to 800°C, as expected. This weight loss most likely corresponds to the water absorbed on surfaces rather than water located between the galleries but indicates that this material is also somewhat hygroscopic.

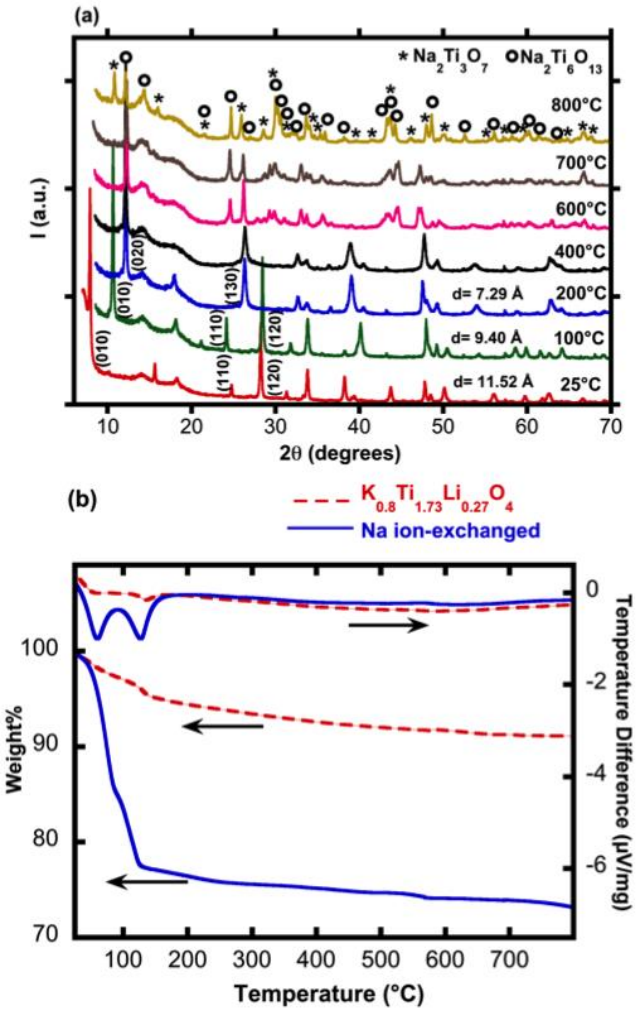

Figure 5. (a) *In situ* XRD patterns of the Na ion-exchanged sample at different temperatures during heating in air. The interlayer distance (d) is calculated from the position of the low angle peak (010) or (020). (b) TG-DTA curves of the $K_{0.8}Ti_{1.73}Li_{0.27}O_4$ and Na ion-exchanged samples heated in air at a rate of 10 °C/min.

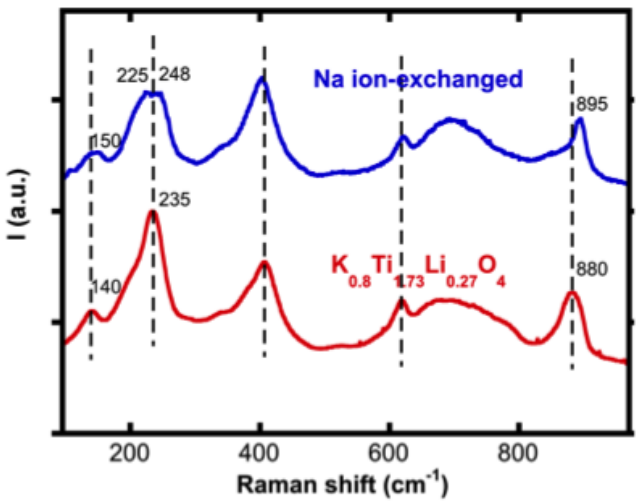

Figure 6. Raman spectra of the $K_{0.8}Ti_{1.73}Li_{0.27}O_4$ and Na ion-exchanged samples.

The Raman scattering spectra of the $K_{0.8}Ti_{1.73}Li_{0.27}O_4$ and the Na ion-exchanged samples (Figure 6) have similar basic features, originating from the corrugated TiO_6 octahedral layers. However, differences are also noticeable, especially in the high wave number region. The peak at high frequency is attributed to the short Ti-O stretching vibration with non-bridging oxygen atoms coordinated to the interlayer cation.[25] This peak is located at higher frequencies for the sodium form compared to the potassium one, shifting from 880 to 900 cm^{-1}, meaning that the bond has become shorter. In addition, the peak at 235 cm^{-1} which corresponds to the Ti-O-K vibration[26] in $K_{0.8}Ti_{1.73}Li_{0.27}O_4$ changed after the ion exchange and split into several overlapping peaks in the Na ion-exchanged sample. These vibrational features are indicative of local structural changes induced by differences in the interactions between the interlayer cations and the octahedral layers. The Raman spectra for the hydrated and dehydrated sodium ion-exchanged materials were identical (not shown).

Electrochemical Characterization

The electrochemical performance of $K_{0.8}Ti_{1.73}Li_{0.27}O_4$ and the sodium ion-exchanged samples dried at 160 ºC and at 250 ºC were evaluated in sodium and lithium coin cell configurations. The electrochemical performance of the C-type sodium ion exchanged material dried at 250 ºC in sodium cells was very poor and is not shown or discussed further in this work. We speculate that the relatively small interlayer spacing in this material creates bottlenecks that interfere with cation diffusion. Figures 7 a and b show the first two charge and discharge profiles and Figures 7c and d the cycling performances of composite electrodes containing $K_{0.8}Ti_{1.73}Li_{0.27}O_4$ or the P-type Na ion-exchanged sample dried at 160 ºC ($Na_{0.8}Ti_{1.73}Li_{0.27}O_4$), at a current density of 0.2 mA/cm^2 between 0.1 and 2.0 V in sodium and lithium half-cell configurations. The $K_{0.8}Ti_{1.73}Li_{0.27}O_4$ electrode delivered an initial discharge capacity of about 200 mAh/g in the lithium half-cell, of which 100 mAh/g was recovered on the first charge. In the sodium half-cell configuration, this electrode showed lower initial discharge and charge capacities of 110 mAh/g and 25 mAh/g, respectively. Because of the very low potentials at which redox activity is observed for the lepidocrocite titanates in both types of cells, there are irreversible side reactions such as insertion of alkali metal cations into the carbon additive in the composite electrode and solid electrolyte interface (SEI) formation[9, 27] that contribute to the initial discharge capacity and the first cycle coulombic inefficiencies. This complicates interpretation of the electrochemical data and makes it somewhat difficult to assess the true insertion capabilities of the electrodes. Values obtained during the first charge give a better assessment of the true reversible capacities of the electrodes than those obtained upon discharge because they are not complicated by these irreversible side reactions.

The theoretical capacity of $K_{0.8}Ti_{1.73}Li_{0.27}O_4$ is most likely limited by its structure, because 40% of the available trigonal prismatic sites are already occupied by potassium ions. Assuming that reduction of Ti^{4+} to Ti^{3+} occurs during discharge and that 60% of the sites are available for insertion of alkali metal cations, the theoretical capacity is estimated to be about 180 mAh/g. However, this can be achieved only if the vacant trigonal prismatic sites can accommodate the intercalated ions without repulsion, since the potassium ions are only 1.5 Å apart. The low mobility of the large and heavy potassium ions also may make rearrangement to accommodate the inserted ions difficult. The smaller size of lithium ions compared to sodium means that more can be accommodated into the structure given these constraints. The sites for lithium probably also differ. Estimating from the first cycle charge capacities, about 60% of the available sites in $K_{0.8}Ti_{1.73}Li_{0.27}O_4$ can be filled with lithium ions (100 mAh/g), but only 15% with sodium (25 mAh/g). In spite of the limited capacities, reasonably good cycling and coulombic efficiencies were achieved after the first cycle for both systems.

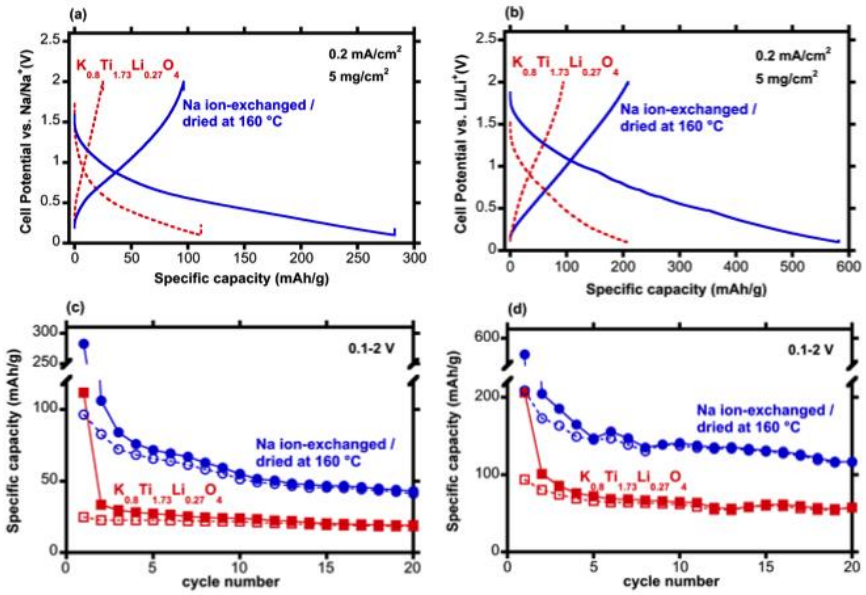

Figure 7. Voltage profiles and cycling data for $K_{0.8}Ti_{1.73}Li_{0.27}O_4$ and Na ion-exchanged/dried at 160 °C ($Na_{0.8}Ti_{1.73}Li_{0.27}O_4$) versus (a,c) Li^+/Li and (b,d) Na^+/Na, cycled at 0.2 mA/cm^2 between 0.1 V and 2 V. Solid symbols show the specific discharge capacity and open symbols show the specific charge capacity values.

In comparison, the sodium ion exchanged electrode material dried at 160 °C showed considerably enhanced discharge/charge capacities in both the lithium and sodium cell configurations (Figure 7). Charge capacities of 200 mAh/g versus Li^+/Li and 100 mAh/g *vs* Na^+/Na were obtained on the first cycle. The relatively large cubic cavities and the replacement of the bulky potassium ions with smaller sodium ones mean that this structure is less severely site limited than $K_{0.8}Ti_{1.73}Li_{0.27}O_4$, and this is reflected in the electrochemical performance. Because some sites are already occupied with sodium ions, the theoretical capacity of $Na_{0.8}Ti_{1.73}Li_{0.27}O_4$ for sodium is estimated to be 192 mAh/g, higher than what is observed experimentally upon recharge. However, sites for the smaller lithium ions may be different than

for sodium, so that it could be possible to insert more lithium than sodium into the structure reversibly. The sites for inserted sodium and lithium ions are currently unknown for these lepidocrocite-type structures, but are likely to be affected both by the overall symmetry and the locations and types of alkali metal cations already present between the layers. As a comparison, a recent neutron diffraction study comparing the structures of $Na_2Ti_6O_{13}$ and $Li_2Ti_6O_{13}$ (prepared by ion-exchange from the sodium-containing precursor) show that Na ions are located in cubic sites in the tunnels whereas the smaller Li ions are shifted and have planar coordination to four oxygens instead.[28] If there were no site limitations at all, the theoretical capacity would be about 275 mAh/g based on reduction of all the Ti^{4+} to Ti^{3+}. Discharges carried out at lower current densities (Figure 8) showed that the higher value was obtained in the lithium cells. In contrast, low rate discharge and charge in sodium cells did not result in an increase in the practical capacity of $Na_{0.8}Ti_{1.73}Li_{0.27}O_4$ for sodium intercalation, providing further evidence that the insertion at higher current densities is limited by the number of sites, rather than by the kinetics as is the case for lithium.

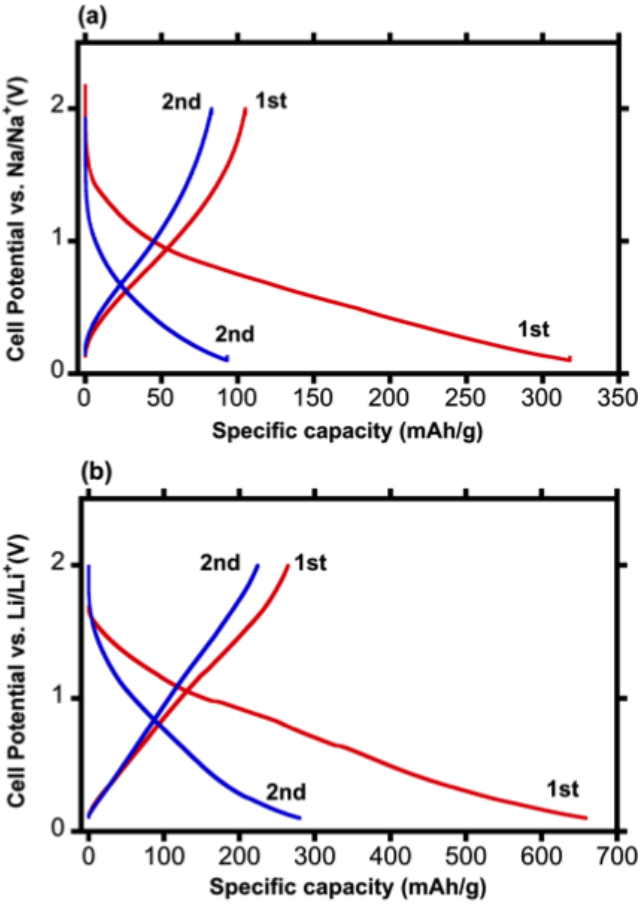

Figure 8. Voltage profiles of (a) sodium half-cells and (b) lithium half-cells containing Na ion-exchanged/dried at 160 °C ($Na_{0.8}Ti_{1.73}Li_{0.27}O_4$) cycled at 0.06 mA/cm^2 between 0.1 V and 2 V.

Evidence of capacity fading was found upon cycling, which was more severe in the case of sodium (Figure 7). This fading could be, in part, due to the very low voltage cutoffs of 0.1V used in these experiments; under these conditions the electrode active material may undergo structural degradation either due to strain or due to over-reduction, and electrolyte decomposition may be exacerbated. To test this theory, the effect of changing the lower voltage limit on the cycling behavior for the two types of cells is shown in Figures 9 a-b (sodium) and c-d (lithium). Although raising this limit from 0.1 V to 0.3V or 0.5 V lowers the initial capacities in both the

sodium and lithium cells, the coulombic efficiencies are improved, particularly in the case of sodium (compare the efficiency of 0.4 or less for the 0.1 and 0.3V cutoffs to more than 0.6 when using 0.5V). The capacity retention is also better; the sodium cell discharged to 0.5V actually has a slightly higher specific discharge capacity than those of the ones discharged to 0.1V or 0.3V by the twentieth cycle. These results suggest that degradation of the $Na_{0.8}Ti_{1.73}Li_{0.27}O_4$ electrode and/or decomposition of the electrolytic solution occurred during discharge to very low potentials.

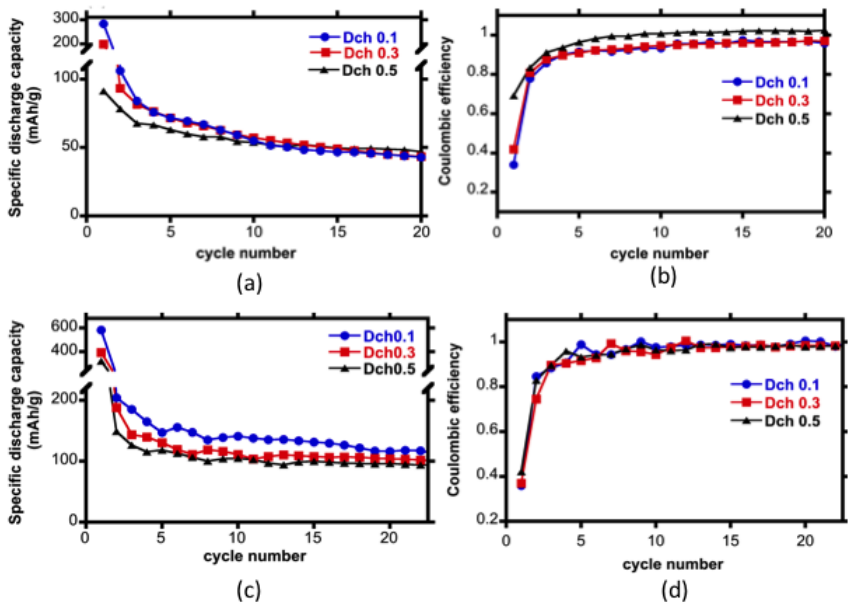

Figure 9. Cycling data and coulombic efficiency data for (a-b) Na cells, and (c-d) Li cells containing $Na_{0.8}Ti_{1.73}Li_{0.27}O_4$ (Na ion-exchanged/dried at 160 °C) electrodes discharged and charged at 0.2 mA/cm^2 to the voltage limits (0.1, 0.3, or 0.5V) indicated on the graphs.

Electrochemical impedance spectroscopy (EIS) was performed on lithium and sodium half-cells at open circuit potential (OCP), and at the end of selected discharges and charges

during cycling at C/5 rate between 2.0-0.1V, to further elucidate the sources of performance degradation. The cycling data for these cells is shown in Figure S1. As in Figure 7, the sodium cell exhibited rapid capacity fading under these conditions. While the lithium cell also deteriorated in performance during initial cycles, the discharge capacity stabilized at about 140 mAh/g by the fifteenth cycle, and no further fading was observed up to the fiftieth cycle, at which point the experiment was terminated. Nyquist plots showing the impedance data at OCP and at the end of discharge and charge for the sodium and lithium cells are given in Figure S2 a-d. The plots consisted of two semicircles and a spur at low frequencies and could be fitted using an equivalent circuit consisting of three components, R1, R2||Q2, and R3||Q3 (labeled in Figure S2b). R1, the high frequency intercept with the real axis, corresponds to the ohmic resistance of the cell components (e.g., electrodes, separator, electrolytic solution, hardware, etc.) and did not vary with cycle number or state-of-charge for the two different cells. The high frequency semicircle (R2) is associated with the solid electrolyte interface (SEI) or reaction layer on the surface of the alkali metal anode, while the low frequency one (R3) is related to properties of the composite positive electrode such as charge transfer resistance and electronic and ionic conductivity. [9, 27] For the lithium cells, R3 was low, particularly at the end-of-discharge, and decreased slightly upon cycling, while R2 changed very little, indicating that the SEI on the surface of the lithium electrode was stable. In contrast, both R2 and R3 increased dramatically upon cycling for the sodium cells, particularly at the end of charge (Figure 10). This shows that impedance increases associated with the sodium-electrolytic solution interface and of the composite electrode itself occurred during cell cycling and were most likely responsible for the observed capacity fading. The increase in R2 upon cycling appears to be specific to this

particular system, since sodium cells containing an electrode derived from $NaTi_3O_6(OH)•2H_2O$ cycled under similar conditions in a previous study did not exhibit the same behavior.[9]

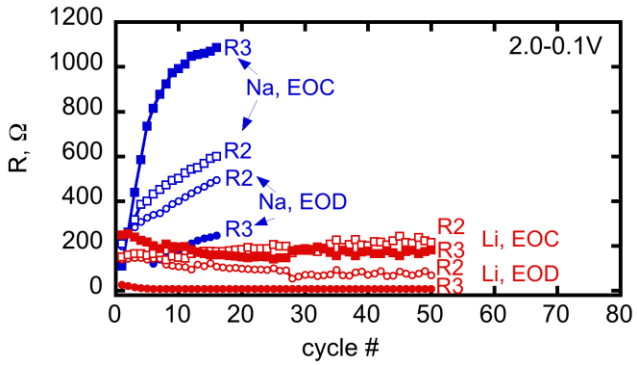

Figure 10. R2 and R3 for lithium and sodium cells containing $Na_{0.8}Ti_{1.73}Li_{0.27}O_4$ (Na ion-exchanged/dried at 160 °C) electrodes, 2 cm^2 in area, as a function of cycle number and state-of-charge (EOC=end of charge, EOD=end of discharge).

The large increases in R3 observed on cycling of the sodium cell indicates that deterioration of the composite lepidocrocite electrode occurred during cycling, although the exact causes cannot be determined from these data alone. Possibilities include degradation of the lepidocrocite phase during insertion and de-insertion processes with formation of inactive impurity phases, formation of increasingly resistive and/or thicker reaction layers on particle surfaces during cycling, and/or disconnection of electronic pathways and isolation of active material in the composite electrode due to large volume changes induced by insertion/de-insertion reactions. Sodium intercalation processes involve larger volume changes than the corresponding lithium insertion ones due to the larger ionic radius of the former (Li^+: 0.76 Å, Na^+: 1.02 Å).[29] This may make sodium intercalation systems more prone to losses due to

mechanical degradation of composite electrodes than the corresponding lithium ones, even if the intercalation processes are chemically reversible.

Results on cells containing electrodes made with polyacrylic acid (PAA) binders suggest that simple mechanical degradation of the composite electrode may indeed be a factor in the performance deterioration of the sodium cells (Figure 11). The incorporation of rubbery binders such as polyacrylic acid (PAA) or carboxymethylcellulose (CMC) has been found to improve the cyclability of electrodes exhibiting large volume changes during lithiation reactions, such as Si[30] and other alloy[31] anode materials in lithium ion systems. These more compliant binders hold the composite electrode together better than the more commonly used PVdF, which tends to crack if a large expansion of the active material occurs. This phenomenon then leads to capacity loss due to electronic disconnection and isolation of active material. A comparison of the data for the $Na_{0.8}Ti_{1.73}Li_{0.27}O_4$ electrodes made with PVdF and PAA binders in sodium cells discharged between 2.0-0.1V at moderate rates (equivalent to approximately C/5) in Figure 11, shows that much better performance is obtained with the latter. The discharge capacity of more than 140 mAh/g obtained during the second discharge of the former was more than 70% of the theoretical value for $Na_{0.8}Ti_{1.73}Li_{0.27}O_4$, compared to a little more than 100 mAh/g for the latter. This strongly suggests that structural degradation of the composite electrode was at least partially responsible for the large decrease in discharge capacity from the first to the second cycle and subsequent fading in the cell containing the electrode made with PVdF binder.

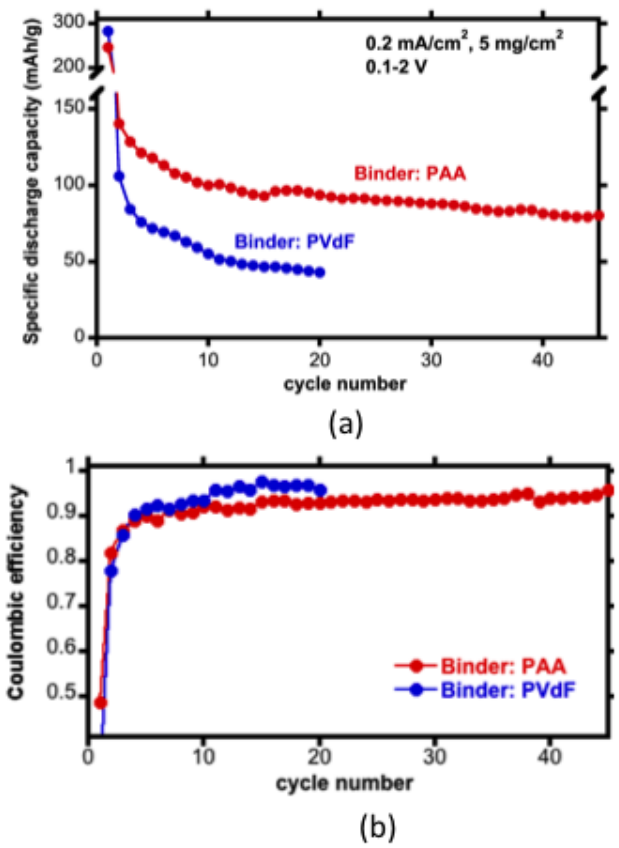

Figure 11. Cycling data (a) and coulombic efficiency (b) for sodium cells containing $Na_{0.8}Ti_{1.73}Li_{0.27}O_4$ (Na ion-exchanged/dried at 160 °C) electrodes prepared with PVdF or PAA binders, discharged and charged at 0.2 mA/cm^2 between 0.1 and 2V.

Ex situ Synchrotron XRD Experiments-Sodium Cells

To investigate the mechanism of the reactions, including possible irreversibilities, *ex situ* synchrotron XRD experiments were carried out on electrodes containing the sodium ion-exchanged material dehydrated at 160 °C, harvested from sodium cells that were discharged to different voltage limits, as well as on electrodes that were recharged. Figure 12a shows selected areas of the XRD patterns of electrodes taken from the sodium cells. Reflections attributable to

the sodium ion exchanged material in the XRD pattern of the pristine electrode had low intensities and were broadened compared to what was observed in the *in situ* heating experiments shown in Figure 5a, in spite of the use of the very bright synchrotron radiation. The low angle region shows two broad low intensity (010) reflections, attributable to the dehydrated $Na_{0.8}Ti_{1.73}Li_{0.27}O_4$ phase and a second hydrated phase with d-spacings similar to the as-made material prior to drying at 160 ºC. The (110) peak of the pristine material is also doubled and the (120) peak is very broad, suggesting that it, too, is duplicated. It is worth noting that a great deal of care was taken to avoid exposure of the electrode to moisture or air during processing; e.g, powders were ground under Ar gas, and Kapton films were used to cover electrodes to prevent exposure to atmosphere before and during the synchrotron experiments. Most likely, the dehydrated phase took up adventitious water during preparation of the slurry used to make the electrodes. Such water was not fully removed during the subsequent drying steps because the presence of the polymeric binder limited the temperature at which the electrodes could be dried to below the dehydration temperature (see Figure 5). This partial re-uptake of water resulted in separation into two related phases, both of which appear to be quite disordered, resulting in the attenuation of peaks.

There was very little change in the pattern for the electrode discharged to 1V compared to the pristine state, but the (010) peak for the dehydrated phase shifted strongly to the left when discharged to 0.5V, while the same reflection in the hydrated one moved only slightly to the right. The insertion of large sodium ions during the discharge process should result in an increase in the interlayer spacing, as indeed occurred for the dehydrated phase. The hydrated phase, in contrast, actually contracted slightly in the *b* direction, suggesting that water was expelled upon insertion of sodium ions. Upon further reduction, a single sodiated phase appeared, as evidenced

by the appearance of only one (010) reflection in the patterns taken on electrodes discharged to 0.1 or 0.3V. This indicates that the product of sodium intercalation into the hydrated phase is identical to that of the dehydrated phase at these potentials. This reflection increased greatly in intensity and sharpness as the reduction progressed, implying increased order in the *b*-direction. The interlayer spacing in this compound is larger than in the pristine dehydrated phase, but much smaller than in the hydrated one, indicating that it is no longer a bilayer arrangement in the galleries (Figure 12b).

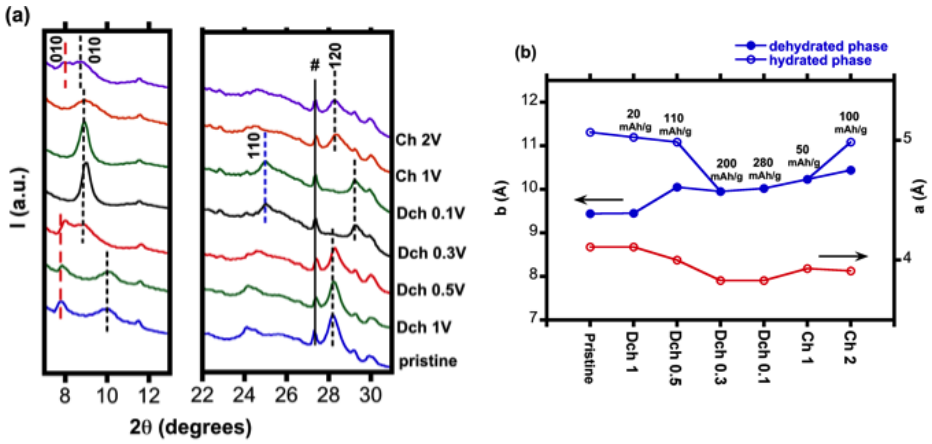

Figure 12. (a) *Ex situ* XRD pattern of $Na_{0.8}Ti_{1.73}Li_{0.27}O_4$ (Na ion-exchanged/dried at 160 °C) electrodes removed from sodium half-cells and discharged or recharged to the indicated voltage limits. (b) *a*- and *b*-lattice parameters of phases formed during discharge and charge of the cells. A peak near 2θ=27° attributable to carbon in the electrode is marked with the symbol #.

The single (010) reflection broadened and became markedly less intense upon recharge to 1V, but did not shift appreciably, even though about 50 mAh/g of charge was extracted from the electrode at this stage. Further desodiation (~100 mAh/g upon charge to 2V) resulted in the splitting of this peak into two broad reflections, with the one at lower angles appearing at approximately the same position as that of the initial hydrated phase. Water molecules that de-intercalated during the initial sodiation reaction are unlikely to survive the low potentials of the

discharge process. (N. B.: irreversible reduction of water to hydrogen gas may be an additional contributor to the first cycle coulombic inefficiencies observed in these cells). Instead, it is likely that solvent from the electrolytic solution co-intercalated during the charge process, eventually producing a phase whose interlayer spacing is consistent with a somewhat disordered bilayer arrangement of solvent molecules and sodium ions. A second phase with a smaller interlayer spacing was also produced. However, its *b*- lattice parameter is much larger than in the pristine dehydrated material, indicating that it, too, must contain solvent molecules in addition to sodium ions. The relatively low charge density and large interlayer spacing of the sodium-containing lepidocrocite phase in the as-made or recharged state predispose it to intercalation of bulky species such as solvent molecules, which then may be partially or fully replaced by inserted sodium ions during discharge.

These processes appear to be largely reversible because no phases unrelated to $Na_{0.8}Ti_{1.73}Li_{0.27}O_4$ were observed even at deep discharge, with the caveat that amorphous reaction products or small amounts of crystalline impurities are not likely to be detected in these experiments. However, intercalation of large guest species such as solvent molecules or bulky anions can lead to structural degradation, and even exfoliation of layered host materials if the expansion of the host is sufficiently large. In fact, this process has been used to produce single layer nanosheets of lepidocrocite titanates for other applications.[32] An experiment in which $Na_{0.8}Ti_{1.73}Li_{0.27}O_4$ powder was stirred in a large excess of 1M $NaPF_6$ EC-DMC electrolytic solution for five days was carried out. This treatment caused the XRD pattern of the powder to change drastically (Figure S3a) to one resembling a C-type lepidocrocite with an expanded *b*-axis (~17.6 Å). In addition to the shifts, the reflections in this pattern were broadened and less intense than those of the pristine sample. EDS analysis (Figure S3b) shows evidence of the

presence of phosphorus in the exposed sample (most likely coming from the PF_6 anion in the electrolyte) and, surprisingly, a total absence of sodium. While the conditions of the electrolyte exposure experiment were severe, the results suggest that degradation of this phase, due to co-intercalation and lattice expansion during electrochemical cycling, is at least a possibility. This hypothesis would be consistent with the capacity fading seen during deep-discharge cycling of cells containing electrodes with PVdF binders, which are poor at accommodating large volume changes, as well as the observation of improved performance when PAA binders, which are more accommodating, are used.

The changes in the lattice parameters shown in Figure 12b show that the dehydrated sodium-containing lepidocrocite titanate expands about 12% in the *b*-direction during the initial sodiation reaction. Much less variation is seen in the *a*-direction. (Because it was not possible to find an unobstructed hkl reflection with $l \neq 0$, changes in the *c* lattice parameter could not be monitored).

Ex situ Synchrotron XRD Experiments-Lithium Cells

The *ex situ* synchrotron XRD data on the $Na_{0.8}Ti_{1.73}Li_{0.27}O_4$ electrodes discharged and charged to different potentials in lithium cells are shown in Figure 13a. In the XRD patterns of the partially and fully discharged electrodes, several new intense reflections appeared. These new peaks, marked with an asterisk in the Figure, did not match any of the Bragg positions of the original $Na_{0.8}Ti_{1.73}Li_{0.27}O_4$ structure or those belonging to the reduction products found in the sodium cells. This indicates that a new phase was formed upon intercalation of lithium into the structure. The positions and relative intensities of the peaks are reminiscent of a lithium form of lepidocrocite titanate ($Li_{0.8}Ti_{1.73}(H_{0.14}Li_{0.13})O_4 \bullet H_2O$) prepared by ion-exchange and described in

reference 15. This phase has C-type symmetry and two interlayer trigonal prismatic sites per formula unit. Its interlayer spacing (~8.2 Å) is much smaller than that of the analogous sodium-containing compound, consistent with a monolayer arrangement of water and cations in the galleries, rather than the bilayer arrangement observed in the latter. The change from $Na_{0.8}Ti_{1.73}Li_{0.27}O_4$ to the C-type lepidocrocite was already evident in the pattern of the electrode discharged to 1V; the 010 and 120 reflections of the P-type dehydrated and hydrated phases disappeared and were replaced by one set of 020 and 130 peaks belonging to the C-type phase. As the reduction of the electrodes in the lithium cell configuration was carried out to lower voltages, these peaks and others belonging to the new phase all increased greatly in intensity, suggesting a much more ordered structure, similar to what happened during sodium intercalation. During the recharge, the compound did not revert to the original P-type lepidocrocite structure of the original sodiated material, although the intensities of the reflections due to the new phase decreased considerably.

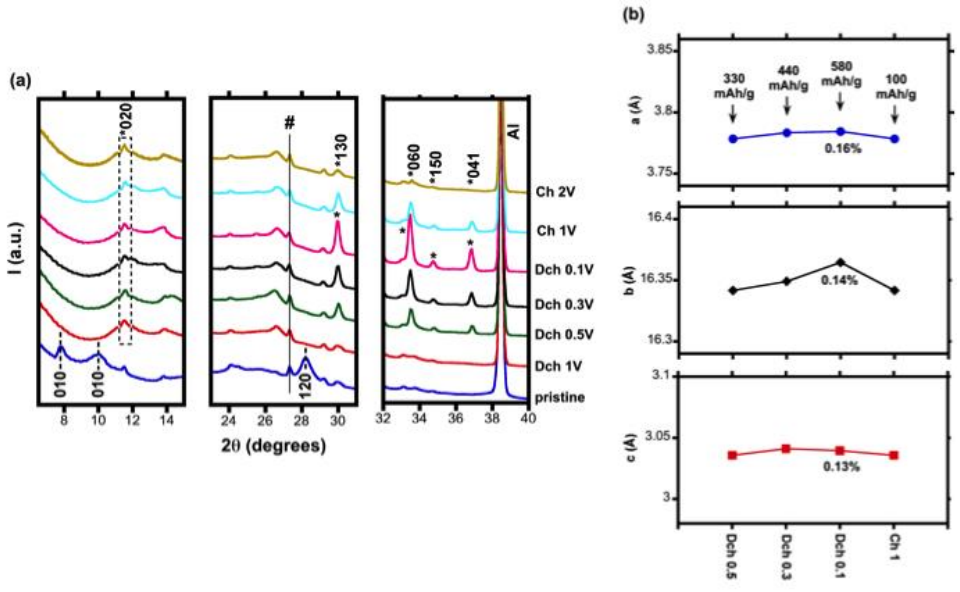

Figure 13. (a) *Ex situ* XRD pattern of $Na_{0.8}Ti_{1.73}Li_{0.27}O_4$ (Na ion-exchanged/dried at 160 °C) electrodes removed from lithium half-cells and discharged or recharged to the indicated voltage

limits. (b) *a*, *b*, and *c*-lattice parameters of phases formed during discharge and charge of the cells. A peak near 2θ=27º due to the carbon conductive additive in the electrode is marked with the symbol #.

The interlayer spacing differences between the hydrated and dehydrated starting materials and the lithium lepidocrocite structure in the fully charged state are large; -27% and -13%, respectively. However, once the C-type structure is formed, the lattice parameter changes are very small (Figure 13b), ranging from ~0.13% - 0.16% in the *a*- , *b*- and *c*-directions between the fully discharged and the fully recharged materials. The interlayer spacing of ~8.2 Å for the charged material is consistent with a monolayer arrangement of cations and solvent molecules, as with the example of $Li_{0.8}Ti_{1.73}(H_{0.14}Li_{0.13})O_4 \bullet H_2O$ given above. The fact that it is nearly invariant with state-of-charge is suggestive of a cooperative mechanism during charge and discharge, in which solvent molecules take the place of the de-intercalated cations and *vice versa*, similar to what happens with $Na_{0.8}Ti_{1.73}Li_{0.27}O_4$ in sodium cells, although only monolayer structures are formed in the case of lithium.

The very small volume changes associated with the redox reactions of the lithium lepidocrocite structure explain the better cycling behavior in lithium compared to sodium cells when PVdF binders are used (Figure 9b and e), regardless of the voltage limit. The large change associated with the ion-exchange and conversion from a P-type to a C-type may, however, contribute to the large first cycle inefficiencies observed in the lithium cells: as shrinkage occurs during the first discharge and ion exchange processes, fresh surfaces are exposed that react with electrolytic solution irreversibly to form an SEI layer. If this is true, performing an *ex situ* lithium ion exchange for the potassium ions in $K_{0.8}Ti_{1.73}Li_{0.27}O_4$ prior to incorporation in lithium cells

should reduce the coulombic inefficiency observed on the first cycle considerably. These experiments will be carried out in our laboratory in the near future.

Conclusions

Lepidocrocite-type potassium titanate $K_{0.8}Ti_{1.73}Li_{0.27}O_4$ was prepared by a solid-state reaction, and a sodium form of this compound was made using a direct ion exchange step. A significant enhancement of the electrochemical capacities was observed for the sodiated structure in both lithium and sodium ion cells due to changes in the site symmetries and the replacement of large potassium ions with smaller sodium ones. Practical capacities of about 140 mAh/g for this compound could be cycled in sodium cells that utilized a compliant binder in the composite anode, close to the theoretical value based on considerations of site availability. In lithium cells, the full theoretical value of 275 mAh/g based on complete reduction of Ti^{4+} to Ti^{3+} could be obtained on the second cycle at low current densities and about 120-150 mAh/g could be cycled at moderate rates (C/5), depending on the lower voltage limit that was used. *Ex situ* XRD studies of electrodes discharged and charged in sodium and lithium cells suggest that redox occurs by a complex solid solution mechanism involving the replacement of de-intercalated sodium or lithium ions with solvent molecules during charge, which minimizes the volume changes associated with this process. The very low potentials at which ion insertion occurs for the lepidocrocite structures have important implications for energy density and cell and electrode design, but appear to be typical for sodium titanate compounds with stepped layered or corrugated structures.

Supporting Information Available. This information is available free of charge via the Internet at http://pubs.acs.org/.

Acknowledgments

This work was supported by the Laboratory Directed Research and Development Program of Lawrence Berkeley National Laboratory under U.S. Department of Energy Contract DE-AC02- 05CH11231. Portions of this research were carried out at the Stanford Synchrotron Radiation Lightsource, a Directorate of SLAC National Accelerator Laboratory and an Office of Science User Facility operated for the U.S. Department of Energy Office of Science by Stanford University.

References

1. Fuse, Y.; Ide, Y.; Ogawa M. *Polym. Chem.* **2010**, *1*, 849.

2**.** Ide, Y.; Ogawa, M.; Angew. *Chem.-Intl Ed.* **2007**, *46*, 8449.

3**.** Dongjiang, Y.; Zhanfeng, Z.; Hongwei, L.; Huaiyong, Z.; Xuebin, K.; Yao, X.; Wu, D.; Sun, Y. *J. Phys. Chem. C* **2008**, *112*, 16275.

4. Behrens, E. A.; Sylvester, P.; Clearfield, A. *Environ. Sci. & Tech.* **1998,** *32*, 101.

5. Osada, M.; Ebina, Y.; Funakubo, H.; Yokoyama, S.; Kiguchi, T.; Takada, K.; Sasaki, T. *Adv. Mater.* **2006**, *18*, 1023.

6. Kudo, A.; Kondo, T. *J. Mater. Chem.* **1997**, *7*, 777.

7. Senguttuvan, P.; Rousse, G.; Seznec, V.; Tarascon, J.-M.; Palacin, M. R., *Chem. Mater.* **2011**, *23*, 4109.

8. Rudola, A.; Saravanan, K.; Mason, C. W.; Balaya P. *J. Mater. Chem. A* **2013**, *1*, 2653.

9. Shirpour, M.; Cabana J.; Doeff M. *Energy & Environ. Sci.* **2013,** *6*, 2538.

10. Pan, H.; Lu, X.; Yu, X.; Hu, Y.-H.; Li, H.; Yang, X.Q.; Chen, L. *Adv. Funct. Mater.* **2013**, *3*, 1186.

11. Rousse, G.; Arroyo Y De Dompablo, M. E.; Senguttuvan, P.; Ponrouch, A.; Tarascon, J.-M.; Palacin, M.R. *Chem. Mater.* **2013**, *25*, 4946.

12. Stevens, D. A.; Dahn, J. R. *J. Electrochem. Soc.* **2000**, *147*, 1271.

13. Sanchez, C.; Rozes, L.; Ribot, F.; Laberty-Robert, C.; Grosso, D.; Sassoye, C.; Boissiere, C.; Nicole L. *Comptes Rendus Chim*. **2010,** *13*, 3.

14. Clearfield, A. *Chem. Rev.* **1988**, *88*, 125.

15. Sasaki, T.; Kooli, F.; Iida, M.; Michiue, Y.; Takenouchi, S.; Yajima, Y.; Izumi, F.; Chakoumakos, B. C.; Watanabe, M. *Chem. Mater.* **1998**, *10*, 4123.

16. Gao, T.; Fjellvag, H.; Norby, P.; *J. Mater. Chem.* **2009**, *19*, 787.

17. Groult, D.; Mercey, C.; Raveau, B. *J. Sol. State Chem.* **1980**, *32*, 289.

18. Reid, A. F.; Mumme, W. G.; Wadsley A. D.; *Acta Crystallogr. B* **1968**, *B 24*, 1228.

19. Sasaki, T.; Watanabe, M.; Michiue, Y.; Komatsu Y.; Izumi, F.; Takenouchi, S. *Chem. Mater.* **1995**, *7*, 1001.

20. England, W. A.; Goodenough, J. B.; Wiseman, P. J. *J. Sol. State Chem.* **1983**, *49*, 289.

21. Larson, A. C.; Dreele, R. B. V.; *Los Alamos National Laboratory Report LAUR*, 1994.

22. Toby, B. H. *J. Appl. Crystallogr.* **2001**, *34*, 210.

23. Lande, J.; Webb, S. M.; Mehta, A. *Area Diffraction Machine*, http://code.google.com/p/areadiffractionmachine/ 2008.

24. Doeff, M. M.; Cabana, J.; Shirpour, M. *J. Inorg. Organometal. Polym. Mater.* **2013**, DOI: 10.1007/s10904-013-9977-8.

25. Bamberger, C. E.; Begun, G. M. *J. Am. Cer. Soc.* **1987**, *70*, C48.

26. Miyaji, F.; Yoko, T.; Kozuka, H.; Sakka, S. *J. Mater. Sci.* **1991**, *26*, 248.

27. Levi, M. D.; Aurbach, D. *J. Phys. Chem. B* **1997**, *101*, 4630.

28. Kataoka, K.; Awaka, J.; Kijima, N.;Hayakawa, H.; Ohshima, K.-I.; Akimoto, J. *Chem. Mater.* **2011**, *23*, 2344.

29. Shannon, R.D, *Acta Cryst.* **1976**, *A32*, 751.

30. Magasinski, A.; Zdyrko, B.; Kovalenko, I.; Hertzberg, B.; Burtovyy, R.; Huebner, C. F.; Fuller, T. F.; Luzinov, I.; Yushin, G. *ACS Appl. Mater. & Interfaces* **2010**, *2*, 3004.

31. Li, J.; Le, D.-B.; Ferguson, P. P.; Dahn, J. R. *Electrochim. Acta*, **2010**, *55*, 2991.

32. Sasaki, T.; Watanabe, M.; Hashizume, H.; Yamada, H.; Nakazawa, H. *J. Am. Chem. Soc.* **1996**, *118*, 8329.

Table of Contents/Abstract Graphic